Journal Pre-proof

Stable carbon isotope ratios of pristine carbohydrates preserved within nannofossil calcite

Harry-Luke Oliver McClelland, Renee B.Y. Lee, Ann Pearson, Rosalind E.M. Rickaby

PII: S0016-7037(24)00462-9
DOI: https://doi.org/10.1016/j.gca.2024.09.007
Reference: GCA 13551

To appear in: *Geochimica et Cosmochimica Acta*

Received date : 20 February 2024
Accepted date : 3 September 2024

Stable carbon isotope ratios of pristine carbohydrates preserved within nannofossil calcite

Harry-Luke Oliver McClelland[a], Renee B Y Lee[b], Ann Pearson[c], Rosalind E M Rickaby[d]

[a]*Department of Structural and Molecular Biology, UCL, London, UK*
[b]*School of Biological Sciences, University of Reading, Reading, UK*
[c]*Department of Earth and Planetary Sciences, Harvard University, Cambridge, USA*
[d]*Department of Earth Sciences, University of Oxford, Oxford, UK*

Abstract

The geochemical characterization of phytoplankton-derived organic compounds found in marine sediments has been widely used to reconstruct atmospheric pCO_2 thoughout the Cenozoic. This is possible owing to a well-established relationship between the carbon isotope ratios of phytoplankton biomass and CO_2 concentration in the ambient seawater. An ideal molecular target for such proxy reconstructions would be degradation resistant on geologic timescales and unambiguously associated with known, experimentally tractable, organisms, so that species-specific models can be developed, calibrated, and applied to appropriate material. However, existing organic matter targets do not quite meet these criteria, primarily owing to ambiguity in the source species of recalcitrant compounds in deep time. Here we explore the potential of a novel organic carbon target for isotopic analysis: acidic polysaccharides extracted from the calcite plates (coccoliths) that are produced by all calcifying haptophytes. Carbohydrates are usually rapidly remineralized in sediments, but coccolith-associated polysaccharides (CAPs) are mechanically protected from diagenesis within the coccolith calcite lattice. Coccoliths can be taxonomically separated by size and identified, often to species level, prior to CAP extraction, providing a species-specific record. Coccolith morphology and composition are important additional sources of information, which are then unambiguously associated with the extracted CAPs. We find that carbon isotope ratios of CAPs changed in response to the environmental changes associated with a glacial cycle, which we attribute to temperature-driven changes in average growth rate. Once the underlying biosynthetic processes and the associated isotope effects are better understood, this archive of pristine organic matter has the potential to provide insight into phytoplankton growth rates and atmospheric pCO_2 far beyond the Cenozoic, to when the first coccolithophores inhabited the surface ocean over 200 million years ago.

Keywords: Carbon isotopes, CO_2 proxies, acidic polysaccharides, coccolithophores, alkenones

1. Introduction

Stable isotope ratios (^{13}C:^{12}C) of organic carbon from ancient marine sediments have long been used to investigate Earth's past environments (e.g. Arthur et al., 1985; Dean et al., 1986; Hayes et al., 1987; Rau et al., 1991; Hayes, 1993; Hayes et al., 1999; Falkowski, 1991; Pearson, 2010; Ward and Shih, 2019; Karhu and Holland, 1996; Hayes and Waldbauer, 2006; Pagani et al., 1999, 2005; Zhang et al., 2013; Freeman and Hayes, 1992). The basis of Cenozoic pCO_2 reconstructions is the fractionation of stable carbon isotopes between phytoplankton biomass and ambient CO_2 (ϵ_p), which results from a large isotope effect associated with photosynthetic carbon fixation, modulated by a reservoir effect. Early models of these bioisotopic systems were fairly generic, consisting of a single compartment representing the cytosol (Sharkey and Berry, 1985; Rau et al., 1996; Keller and Morel, 1999; Cassar et al., 2006; Popp et al., 1998), but it has recently been shown that interspecific differences in metabolism and ultrastructure / compartmentation among cyanobacteria and various groups of algae have a marked effect on ϵ_p and must be modeled explicitly (Holtz et al., 2017; Wilkes and Pearson, 2019; Hurley et al., 2021; Phelps et al., 2021). It is therefore essential to know the source of any organic matter analyzed so that isotope data can be interpreted with the appropriate model and experimental calibration. Stable isotope ratios are also subject to diagenetic alteration, which has the potential to bias or corrupt the original signal (Freudenthal et al., 2001). An ongoing challenge to reliable quantitative paleoenvironmental reconstructions is therefore the search for an organic matter target that can be: 1. unambiguously attributed to a particular organism; and 2. whose integrity from deposition to analysis can be assured. In this manuscript we explore a novel organic matter target that has the potential to meet both of these criteria.

ϵ_p is given by:

$$\epsilon_{\mathrm{p}} \equiv 1000\left[\frac{\delta_{\mathrm{CO_2}}+1000}{\delta_{\mathrm{bio}}+1000}-1\right] \approx \delta_{\mathrm{CO_2}}-\delta_{\mathrm{bio}}, \quad (1)$$

where δ values are given in permil (‰). δ_{CO_2} corresponds to the carbon isotopic composition of dissolved CO_2, and δ_{bio} to that of phytoplankton biomass (see Eq.2 for definitions). Phytoplankton biomass is depleted in ^{13}C relative to ambient CO_2, so as defined here ϵ_p is positive, consistent with previous work (Farquhar et al., 1982; Jasper et al., 1994). Empirically ϵ_p increases in magnitude with increasing CO_2 concentration and

Email address: h.mcclelland@ucl.ac.uk (Harry-Luke Oliver McClelland)

decreases with increasing growth rate and cell size (Laws et al., 1995; Bidigare et al., 1997).

In paleoclimate reconstructions δ_{bio} (Eq.1) was originally estimated by analyzing bulk sedimentary marine particulate organic matter (POC) (Hollander and McKenzie, 1991; Freeman and Hayes, 1992). POC has been largely replaced by molecular organic markers, specifically alkenone and, more recently, phytane lipids and their degradation products (Jasper and Hayes, 1990; Pagani et al., 1999; Pagani, 2002; Laws et al., 2002; Pagani et al., 2005, 2011; Seki et al., 2010; Badger et al., 2013; Zhang et al., 2013, 2020; Witkowski et al., 2018, 2019, 2020). Alkenones, a class of putative storage lipids (Conte et al., 1995), are produced in the modern ocean by a single known order of haptophyte algae, the Isochrysidales, which includes the calcifying genus *Gephyrocapsa* (Marlowe et al., 1990) including the cosmopolitan *G. huxleyi* (synonym *Emiliania huxleyi*, Reinhardt, 1972). They are highly degradation-resistant, and found in marine sediments as old as 120Ma (Brassell et al., 2004) (but are increasingly scarce prior to ~ 30 Ma).

Coccoliths, the calcite plates that are produced by calcifying haptophytes (collectively known as coccolithophores), are often preserved in sediment alongside alkenones. All modern Isochrysidales appear to produce alkenones, and the appearance of alkenones in the sedimentary record coincides with the first appearance of coccoliths of this group (Liu et al., 2010), providing a basis for their assumed affiliation on geologic timescales. The morphology of coccoliths can be used to identify the taxonomic affinity of the source organism (Young et al., 2017) and estimate cell size (Henderiks and Rickaby, 2007; Henderiks and Pagani, 2008; Henderiks, 2008), and their trace metal ratios can potentially even provide estimates of growth rate (Stoll and Schrag, 2000; Rickaby et al., 2002; Langer et al., 2006).

However, the confidence with which alkenones in sediment can be attributed to the organisms that produced contemporaneous coccoliths is limited by the fact that cells disintegrate after death, and these components of cellular material are found separately to one another in marine sediments. Non-calcifying species of Isochrysidales, which do not have a fossil record, also contribute to sedimentary alkenones. Furthermore, when multiple species and sizes of Isochrisodales coccoliths are present, attributing their weighted contibution to sedimentary alkenones depends on differences in coccolith preservation (Andruleit et al., 2004) and variations in the number of coccoliths and amount of alkenone lipids produced by different species. These ambiguities, in addition to the observation that alkenones may be transported and recycled differently to other components of sediment (Hayes et al., 1987; Ohkouchi et al., 2002; Mollenhauer et al., 2003) weakens the assumption that the auxillary information derived from coccoliths pertains to the producers of the alkenones in the same samples.

Here we explore the potential of coccolith associated acidic polysaccharides (CAPs) as a novel target for organic carbon isotopic analysis. CAPs are carbohydrates, molecules that are not usually preserved on geologic timescales. In coccolithophores, however, the precipitation of calcite occurs in an intracellular golgi body-derived compartment called the coccolith vesicle (Young, 2003), onto a precursor organic framework consisting of CAPs (Marsh et al., 1992; Marsh, 1994; Marsh et al., 2002). Consequently, CAPs are mechanically preserved inside the crystal lattice of coccolith calcite (Lee et al., 2016). So far, CAPs have been found to be present inside the coccoliths produced by coccolithophores of all taxonomic affinities and ages (at least as old as the Early Jurassic; 184 Ma Lee et al., 2016). Thus CAPs constitute an archive of coccolithophore-associated organic carbon which is unambiguously associated with the source organism, and whose taxonomic diversity and temporal range far exceeds that of alkenones.

The concept for our approach is as follows (Fig. 1): Sediments from sediment core fine fractions are taxonomically separated by size using established techniques (Minoletti et al., 2009; Bolton et al., 2012). The carbon isotope ratios of calcite and of the extracted and purified CAPs are determined for each single size fraction. The carbon isotope values of the CAPs (δ_{CAP}) and the calcite (δ_{cal}) are controlled by different processes, so the fractionation of carbon isotopes between these phases ($\Delta_{cal\text{-}CAP}$) is itself a function of these processes (Fig. 2). $\Delta_{cal\text{-}CAP}$ bypasses the need for a secondary reference (e.g. foraminiferal calcite) for the isotopic composition of CO_2 in seawater. This approach further resolves the ambiguity in the association between the coccoliths (and their associated information) and the organic matter target. Though this approach in principle solves several shortcomings associated with other methods, a number of questions have emerged. In the following we outline the potential, and current limitations, of this approach.

2. Materials and Methods

2.1. Isotope notation

Carbon isotope values are reported as δ values, relative to the VPDB calcite standard. As we only discuss carbon isotopes we use the following shorthand for brevity:

$$\delta_x \equiv 1000\left[\frac{\frac{^{13}C}{^{12}C}_x}{\frac{^{13}C}{^{12}C}_{VPDB}} - 1\right], \tag{2}$$

where the subscript, x, refers to the analyzed phase. Throughout this manuscript we use Δ notation, which is defined as the difference in δ values, and closely approximates ϵ at realistic carbon isotope δ values. The generic form is given as:

$$\begin{aligned}\Delta_{a\text{-}b} &\equiv \delta_a - \delta_b \\ &\approx \epsilon_{a\text{-}b} \equiv 1000\left[\frac{\delta_a + 1000}{\delta_b + 1000} - 1\right],\end{aligned} \tag{3}$$

where a and b refer to different phases. Note ordering of subscripts throughout.

2.2. Size-separation

To investigate changes in coccolithophore carbon isotopes over the penultimate glacial cycle (marine isotope stage; MIS 7-5), we selected twenty samples from ODP Site 1123 including ten samples spaced at higher resolution across the termination (TII). Each sample initially consisted of approximately 5

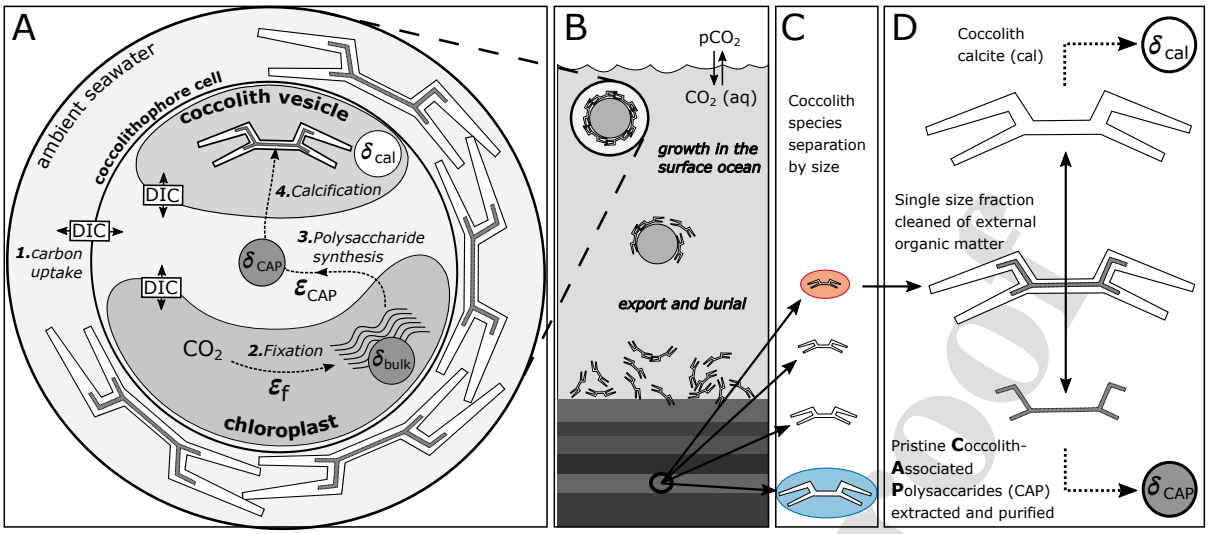

Figure 1: **Schematic of the concept. A:** Carbon fluxes and relevant pools within a coccolithophore cell with four relevant stages: 1. Dissolved inorganic carbon (DIC) enters a coccolithophore cell from the ambient seawater (in the form of CO_2 and bicarbonate), and is redistributed among intracellular compartments; 2. RuBisCO-catalysed CO_2 fixation into organic matter in the chloroplast is associated with a large kinetic isotope effect (ϵ_f). The primary photosynthate is depleted in ^{13}C relative to source CO_2; 3. Acidic polysaccarides are synthesised from simple sugars, and are enriched relative to bulk biomass by an amount ($\epsilon_{CAP\text{-}bio}$); 4. Calcite precipitation occurs in the coccolith vesicle onto a precursor organic framework consisting of acidic polysaccharides (coccolith-associated polysaccharides - CAPs). The CAPs are protected within the calcite crystal, and are stable as long as the calcite is intact. The coccolith is constructed intracellularly, and then is ejected and incorporated in to the extracellular coccosphere. **B:** Coccolithophores grow in the surface ocean, producing organic matter and calcite that have isotopic compositions that reflect cellular physiology and the ambient environment. Coccoliths sink out of the surface ocean (export) and accumulate on the sea floor (burial). Cells do not remain in tact after death, so the calcite coccoliths are usually found in sediment as isolated plates, rather than as fully articulated coccospheres. **C:** Coccoliths in sediment accumulated over time are extracted by drill core and a sediment sample representing a single time interval is separated into near monospecific fractions by size. **D:** Each size fraction is then cleaned of all external organic matter, and the CAPs are extracted and purified. The carbon isotope ratios of the CAPs are analysed together with the encasing calcite.

g of sediment fine fraction (dry weight following wet-sieving at <63 μm). Following qualitative light-microscope taxonomic and morphometric assessment of sample smear slides, we targeted the size fraction within the range 2-3 μm, which consisted of small *Geophrocapsa* spp.. This size fraction was obtained following a combination of differential settling and the microfiltration protocol of (Minoletti et al., 2009). Non-coccolith carbonate debris was rare in the final samples, with intact coccoliths estimated by visual inspection to comprise >95% of the mass of the sample (with the exception of one contaminated sample, which is excluded from further analysis). The final 2-3 μm size fraction was typically 2 g dry weight (~ 40% of total fine fraction). We also generated a 8-12μm fraction, containing pure *Coccolithus pelagicus*. However, due to the relatively low amount of calcite in this pure fraction, the yield of extracted CAP was very low, which resulted in large uncertainties in isotopic values (Fig. 3; CAP:L). The requirement for very large calcite samples presents a significant logistical challenge, due to the difficulty of securing large sediment samples, and the substantial time required for size separation.

2.3. Calcite carbon isotopes

Carbon isotopic compositions of the size-separated calcite were measured using a VG Isogas Prism II mass spectrometer with an on-line VG Isocarb common acid bath preparation system in the Department of Earth Sciences, University of Oxford, UK. Samples were dosed with acetone and dried at 60°C for at least 30 minutes. In the instrument they were reacted with purified phosphoric acid at 90°C. Calibration to PDB standard was via the international standard NBS-19 using the Oxford in-house (NOCZ) Carrara marble standard. Reproducibility of replicated standards was around 0.1‰ for $\delta^{13}C$ (1σ) expressed relative to the VPDB standard.

2.4. CAP extraction

From the size separated samples, 1.000 g (dry weight) of the 2-3 μm fraction was taken for CAP extraction. The 8-12 μm fractions were much smaller but were not weighed prior to CAP extraction. The polysaccharide extraction protocol used here was adapted in Lee et al. (2016) from established protocols (De Jong et al., 1976; Ramus, 1977; Marsh et al., 1992) and comprises the following steps:

1. *Removal of residual external organic matter*: Samples were suspended in 10 ml 1% (v/v) TritonX-100 and 4.5% (v/v) NaOCl in 0.05 M $NaHCO_3$, and gently shaken for 30 minutes. Samples were rinsed thoroughly in de-ionized water (de-ionized to 18.2 MΩ.cm with MilliQ system). Following suspension in 0.05 M NH_4HCO_3, the sample was centrifuged through a gradient of 100 ml Ludox® TM-50 colloidal silica layered with 20% (w/v) sucrose at 23,000 g for 20 min at 4°C. The pellet (containing the clean coccoliths) was rinsed five times with 0.05 M NH_4HCO_3.

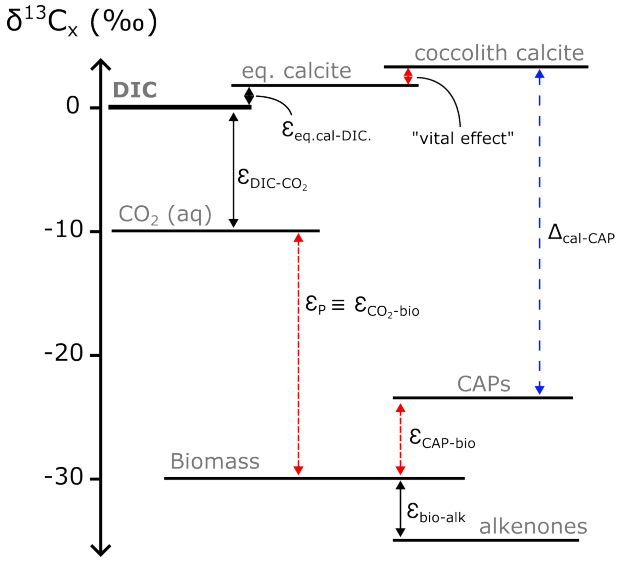

Figure 2: **Outline of approximate δ values of relevant phases.** Fractionations represented by solid black arrows are approximately constant across typical conditions. Fractionations represented by red densely dashed arrows are variable. See text for discussion of "vital effects", which can be positive or negative, and the factors controlling ϵ_p and $\epsilon_{\text{CAP-bio}}$. $\epsilon_{\text{cal-CAP}}$, represented by the blue loosely dashed arrow, represents the net result from several variable fractionations.

2. *Decalcification of cleaned coccoliths and liberation of the CAPs*: The cleaned coccoliths were decalcified with 0.5 M EDTA (pH 8.0) at 4°C for 12 hours, followed by ultrasonication. Following centrifugation at 31,000 g, the insoluble residue, consisting mostly of clays, was discarded.
3. *Isolation and Purfication of CAPs*: The supernatant was buffer exchanged with 20 mM TrisHCl (pH 8.0) using a 10,000 MWCO Amicon Ultra-4 membrane (Millipore) to extract larger organic molecules from the complex salt solution into a stable buffer for subsequent steps. The solution was subjected to anion exchange liquid chromatography (HiTrap DEAE FF, GE Healthcare) according to the manufacturer's protocol, which binds the charged, acidic molecules to the column, and allows any uncharged compounds to flow through. The CAPs were eluted from the column using 0.5 M NaCl, buffer exchanged with MilliQ (10,000 MWCO Amicon Ultra-4 membrane, Millipore) and stored at -20°C.

The pristine condition of CAPs extracted from fossils using this approach is supported by a comparison between CAPs extracted from growing cultures and fossil samples of various ages using reverse-phase high-performance liquid chromatography (RP-HPLC) (Lee et al., 2016).

2.5. CAP carbon isotopes

The purified CAP samples were measured on a Thermo Delta Plus Advantage stable isotope mass spectrometer, with Spooling Wire Microcombustion (SWiM) interface Sessions et al. (2005), at Harvard University. The SWiM interface allows measurement of ng scale samples, and works as follows. A nickel wire is passed through a cleaning oven, which removes organic carbon on the wire and forms the nickel oxide catalyst. A 0.8 μL droplet of sample is placed on the wire before the solvent is evaporated and organic carbon is combusted in a ceramic reactor tube in the presence of a copper and platinum catalyst to form CO_2; water is removed through a Nafion dryer and CO_2 passes through a continuous-flow open split capillary to the isotope ratio mass spectrometer. A more detailed description of the equipment and protocol is given in Sessions et al. (2005). Organic carbon measurements made in Harvard were calibrated for consistency with measurements made in Oxford, using an apple pectin standard in a dilution series.

In addition to blanks used during analysis, three types of process blank were created to test whether contamination is accrued at various points of the CAP extraction and purification protocol. When processed through the protocol outlined in section 2.4, each sample should theoretically yield no carbon:

- Samples of laboratory-grade calcium carbonate, roasted at ~600°C to combust any organic matter present. This blank tests whether organic matter contamination occurs after decalcification with EDTA.
- Sediment fine fractions from the same core as our samples, treated with acid to dissolve the calcium carbonate, and then neutralised and washed. The purpose of this blank is to check that any organic matter in the sample not encased within coccolith calcite is effectively removed prior to decalcification with EDTA.
- Picked, cleaned and crushed foraminifera. This blank tests whether foraminiferal debris (and the organic matter locked inside them) has the potential to contaminate the CAP sample via the extraction and purification protocol described above.

There was no significant difference between the amount and isotopic composition of carbon detected across the analysis blanks and the different process blanks, which suggests that the extraction protocol introduces negligible contamination.

For the isotopic analysis of CAP samples, a mass-balance correction was applied to account for the size and isotopic composition of the background. The size of the sample relative to the size of the blank strongly influences the uncertainty in the final reported δ^{13}C values. If the sizes of sample and blank are similar, the inferred isotope value is also affected. Across the three blanks described above, the concentration of carbon in each droplet introduced to the wire was on average 1.85 *n*molC μL^{-1} (σ = 0.15 *n*molC μL^{-1}). Following dilution to optimal concentrations, the concentrations of CAP suspensions applied to the wire were on average 7.21 *n*molC μL^{-1} (σ = 1.81 *n*molC μL^{-1}) across the small size fraction samples. Across the large size fraction samples the average was 3.75 *n*molC μL^{-1} (σ = 0.91 *n*molC μL^{-1}). Given their lower undiluted concentrations, the large size fraction samples were concentrated with a centrivap and run again to confirm isotopic compositions. The isotopic composition of the blanks was consistently -27±1‰. The 1 standard deviation uncertainty in the isotopic composition of

the sample (σ_{δ_s}) is calculated according to Eq. 5.19 of Hayes (2002):

$$\sigma^2_{\delta_s} = \frac{1}{(n_T - n_b)}\left[\left(\frac{n_b(\delta_b - \delta_T)}{n_T - n_b}\right)^2 \sigma^2_{n_T} + n^2_T \sigma^2_{\delta_T}\right] + \frac{1}{(n_T - n_b)}\left[\left(\frac{n_T(\delta_T - \delta_b)}{n_T - n_b}\right)^2 \sigma^2_{n_b} + (-n_b)^2 \sigma^2_{\delta_b}\right], \quad (4)$$

where n values are molar quantities, and δ values are isotopic compositions, of the total measured sample (subscript, T), the blank (subscript, b) and the true value of the sample (subscript, s). A conservative value of 0.46 was used as the uncertainty in the size of the blank (σ_{n_b}; 25% of the mean size of the three blanks), which is significantly larger than the standard deviation of the size of the blanks. These calculations give the errors shown in Fig. 3.

2.6. Core location and Environmental reconstruction

ODP Site 1123 (Expedition 181) is located on Chatham rise, east of New Zealand in the southernmost Pacific (41°47.2'S, 171°29.9'W, 3290m water depth). In the modern ocean surface ocean, CO_2(aq) at this site is close to equilibrium with atmospheric pCO_2 (Martínez-Botí et al., 2015). We have previously found excellent preservation of coccoliths at this site during the time period studied (McClelland et al., 2016). The sediment age model for ODP Site 1123 was taken from Elderfield et al. (2012a), which was based on a correlation with the orbitally tuned benthic oxygen isotope stack of LR04 (Lisiecki and Raymo, 2005). Owing to the location of Site 1123 just north of the sub tropical front (STF), the site has the potential to see local swings in temperature. We therefore reconstructed sea surface temperatures (SSTs) directly using the alkenone temperature proxy ($U^k_{37'}$) interpreted with the BAYSPLINE model of (Tierney and Tingley, 2018). $U^k_{37'}$ is the best available temperature proxy for our purposes as it captures the depth habitat of coccolithophores.

New sediment samples spanning the range of our coccolith samples were processed for total lipid extracts (TLEs) using a CEM-MARS microwave extraction system with dichloromethane:methanol solvents as described in Polik et al. (2018). The resulting TLEs were stored at -20°C. For analysis, aliquots of the TLEs were dissolved in 97:3 (v/v) hexane:isopropanol, filtered, and analyzed on an Agilent 1290 Infinity series ultra-high-performance liquid chromatography (UHPLC) system coupled to an Agilent 6410 triple-quadrupole mass spectrometer (MS) using atmospheric pressure chemical ionization (APCI). Core GDGT distributions were determined on tandem Acquity BEH HILIC amide columns (2.1 × 150 mm, 1.7 μm particle size, Waters Corporation, Milford, MA) and quantified following the method outlined by Becker et al. (2015) with modifications by Polik et al. (2018).

$U^k_{37'}$ and TEX_{86} calculations were conducted using established methods. TEX_{86} ratios were determined according to the equation of Schouten et al. (2002) and TEX_{86} was converted to SST (°C) using the BAYSPAR model of Tierney and Tingley (2014). The Becker et al. (2015) method also generates simultaneous records of alkenone-derived SSTs ($U^{K'}_{37}$; (Müller et al., 1998)). $U^k_{37'}$ was converted to SST using the BAYSPLINE model of Tierney and Tingley (2018). The TEX_{86} and $U^k_{37'}$ SST reconstructions both reveal similar relative changes throughout the glacial cycle. Owing to the production of alkenones by coccolithophores, and the depth habitat represented by these data, $U^k_{37'}$ SSTs are presented in the main manuscript, and are compared to TEX_{86} SSTs in the supplementary material.

The pCO_{2atm} record is taken from a consensus compilation of CO_2 mixing ratios from a number of Antarctic ice cores (Bereiter et al., 2015), and assumed to represent a well-mixed atmosphere. By assuming equilibrium between the surface ocean and atmosphere, [CO_2(aq)] is estimated from SST and pCO_{2atm} using the *seacarb* package in R (Gattuso et al., 2022), with dissolution assumed to be controlled only by SST at a constant salinity of 35. As CO_2 is more soluble in seawater at low SST, changes in inferred SST that accompany changes in atmospheric pCO_2 result in an offset between pCO_2 and [CO_2(aq)]. The highest value of [CO_2(aq)] occurs at 120 ka when pCO_2 is still high and reconstructed SST falls slightly. All sediment core ages are projected onto the LR04 timescale (Lisiecki and Raymo, 2005), and all gas ages, including pCO_{2atm}, are on the AICC2012 timescale (Bereiter et al., 2015; Bazin et al., 2013). To account for the estimated ~3 ky temporal uncertainty in the alignment of these sediment and gas records, both the pCO_2 and SST records were smoothed with a LOESS filter with a span that acts as a low pass filter with a cut off around 3 ky, prior to combining to calculate [CO_2(aq)].

3. Results

CAPs were successfully extracted from within the calcite comprising the 2-3 μm and 8-12 μm fractions, which we refer to as the *small* and *large* size fractions respectively. For each 1g of size-separated coccoliths (dry weight) from the small size fraction, the final yield was on the order of 5 - 15 μg CAP (~ 165 - 500 nmolC). An approximate yield is around 300 nmolC (CAP) g^{-1} (coccolith calcite). The carbon isotopic compositions of the calcite (δ_{cal}) and of the CAPs (δ_{CAP}) of both size fractions were measured. For the small size fraction δ_{cal} values range from -0.5 to 1.7 ‰$_{VPDB}$ throughout the glacial cycle, while the large size fraction δ_{cal} values range from -2.0 to -0.6 ‰$_{VPDB}$ (Fig. 3). The variation in δ_{CAP} throughout the glacial cycle was somewhat larger with values ranging from -18.4 to -13.8 ‰$_{VPDB}$ in the small size fraction, and -22.2 to -11.8 ‰$_{VPDB}$ in the large size fraction. Both δ_{CAP} records transiently shift towards the most negative values at around 130 ka, coincident with the glacial termination. As the CAP yield for the large size fraction was so low, the uncertainties in δ_{CAP} values are much higher than for the small size fraction, and relative changes in this series should be treated with caution. The δ_{CAP} values of the large size fraction are, however, consistently 3-4 ‰ lower than those of the small size fraction. All raw data are shown in Fig. 3.

We define $\Delta_{cal:S-CAP:S}$ to be the magnitude of the difference between δ_{CAP} and δ_{cal} of the small size fraction, and $\Delta_{cal:L-CAP:L}$ to be the equivalent for the large size fraction (Fig. 3). The

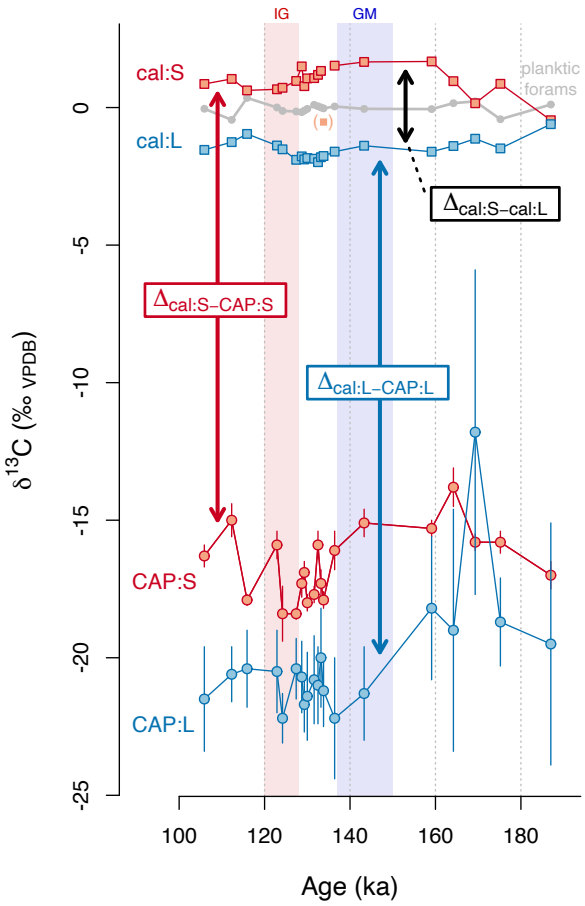

Figure 3: **Raw data.** Time series of carbon isotope compositions of calcite from the 2-3 μm (small) size fraction (cal:S), calcite from the 8-12 μm (large) size fraction (cal:L), CAPs from the small size fraction (CAP:S), and CAPs from the large size fraction (CAP:L). The point in parentheses was contaminated with a larger size fraction but is included here for completeness. Δ values defined as in Eq.3. The blue shaded box highlights the glacial maximum (GM), and the red shaded box highlights the inter-glacial (IG).

fractionation of carbon isotopes between CAPs and calcite is independent of the isotopic composition of extracellular DIC. For comparison with recent literature (Bolton and Stoll, 2013; Bolton et al., 2016; McClelland et al., 2017; Claxton et al., 2022), we also define $\Delta_{cal:S-cal:L}$ to be the difference in δ values for the calcite from the small and large size fractions (Fig. 3). $\Delta_{cal:S-CAP:S}$ has a large range across the glacial cycle with a minimum of 14.8 and a maximum of 19.4, which occurs at around 125-130 ka (Fig. 4). These changes reflect primarily changes in δ_{CAP} as although δ_{cal} in the small size fraction does change, these changes are small and the direction of change dampens rather than amplifies changes in $\Delta_{cal:S-CAP:S}$ (Fig.3). Proxy reconstructions show SSTs ranging from around 10°C at 165 ka to around 14°C at around 130-125 ka, which coincides with the maximum in $\Delta_{cal:S-CAP:S}$ (Fig. 4). [CO_2 (aq)] in surface waters is calculated based on the Antarctic ice-core pCO_2 record and SST, and exhibits a maximum value which occurs around 10ky later than the maximum in $\Delta_{cal:S-CAP:S}$.

4. Discussion

4.1. Controls on carbon isotope fractionation

Traditionally, it has been assumed that the maximum value of ϵ_p is set by the CO_2 fixation step in the Calvin cycle, which is catalyzed by the enzyme Ribulose-1,5-bisphosphate carboxylase/oxygenase (RuBisCO), and is associated with a large normal kinetic isotope effect (ϵ_f). ϵ_f varies between RuBisCO types (reviewed in Wilkes and Pearson (2019)), and between species (Boller et al., 2011, 2015). The modulation of this maximum fractionation has typically been described as an open system reservoir effect, where ϵ_p is a linear function of carbon utilization (Hayes, 2002). The theoretical relationship deviates from linear as more complex features are included in models including: intracellular compartmentalization (Cassar et al., 2006), dynamic carbonate chemistry (Holtz et al., 2017), the presence of carbonic anhydrase (CA) (Holtz et al., 2017), cellular boundary layers (Rau et al., 1996; Riebesell et al., 1993), respiration (Holtz et al., 2017), facultative mixotrophy (Gould et al., 2008; de Vargas et al., 2007), light availability (Rost et al., 2002; Holtz et al., 2017; Wilkes and Pearson, 2019; Phelps et al., 2021) and bicarbonate uptake (e.g. Sharkey and Berry, 1985; Kottmeier et al., 2014; Nimer et al., 1997; Herfort et al., 2002; Nimer et al., 1996; Keller and Morel, 1999; Cassar et al., 2006; Holtz et al., 2017; McClelland et al., 2017; Wilkes and Pearson, 2019).

Here we consider changes in the CO_2 utilization parameter, τ, defined as the ratio of the rate of carbon fixation to CO_2 entering the cell by passive diffusion alone. For a spherical cell of radius r, the rate of fixation of CO_2 into organic matter can be estimated by the product of the cell's volume ($\frac{4}{3}\pi r^3$), it's carbon molar density (ρ), and its instantaneous division rate μ_i (Sharkey and Berry, 1985; Rau et al., 1996; Holtz et al., 2017; Rost et al., 2002). The supply rate of CO_2 delivered by passive diffusion through the membrane is given by the product of the cell's surface area ($4\pi r^2$), the CO_2 concentration at the cell's surface (C_e), and the effective membrane permeability to CO_2 (K) (Popp et al., 1998). Following notation introduced previously (McClelland et al., 2017):

$$\tau = \frac{\mu_i r \rho}{3 C_e K}. \quad (5)$$

In reality diffusive CO_2 is supplemented by various ancillary mechanisms of carbon uptake, so τ does not equate directly to utilization (for example, τ can take a value of greater than 1). Nevertheless, we find this compound variable to be a useful way to consider changes in ϵ_p: An *increase* in τ corresponds to a *decrease* in ϵ_p. We emphasise that quantitative interpretations require a more sophisticated model. Relative to bulk biomass CAPs are enriched in ^{13}C (Fig.2), with a variable offset (see Section 4.2 for discussion).

The fractionation of carbon isotopes between DIC and coccolith calcite is also impacted by biological processes, and is

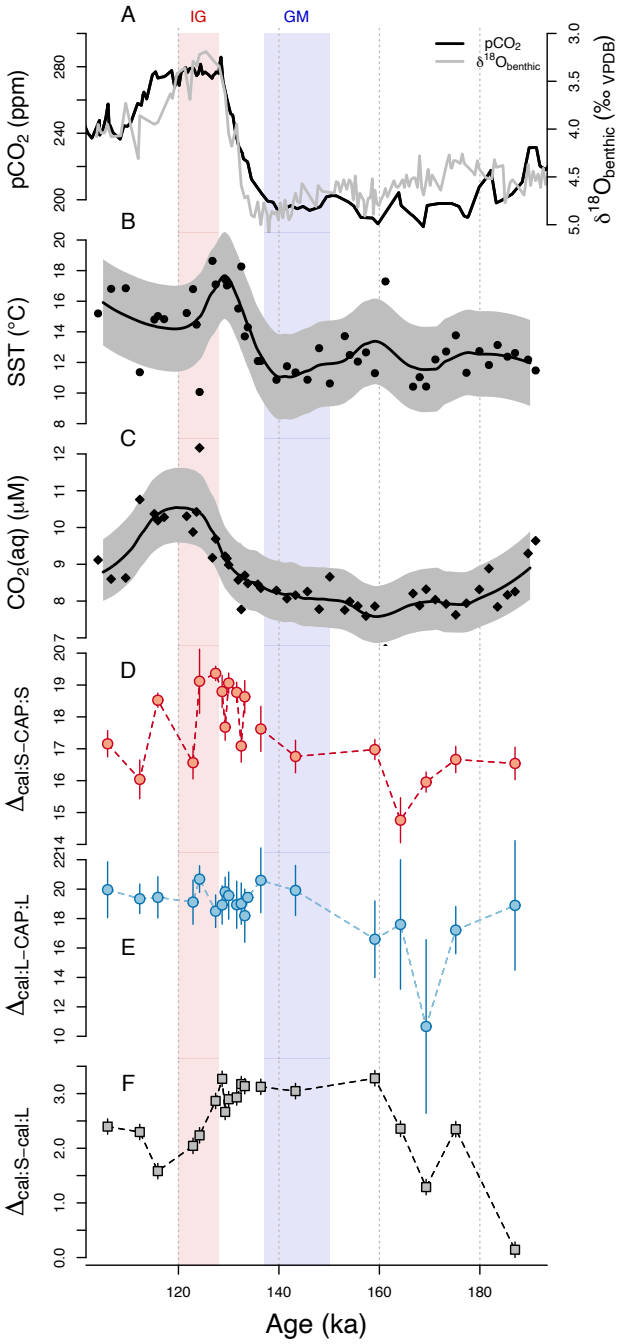

Figure 4: **Proxy data.** **A:** pCO_2 record from Antarctic ice cores (Bereiter et al., 2015), assumed to represent a well-mixed atmosphere. $\delta^{18}O$ of benthic foraminifera shells from ODP Site 1123 (Elderfield et al., 2012b) for visual reference to the LR04 stack (Lisiecki and Raymo, 2005). **B:** SST record derived from $U^{k}_{37'}$. Line represents a LOESS regression, and shaded region represents 1σ uncertainty. **C:** $[CO_2(aq)]$ calculated from SST and pCO_2 assuming surface ocean / atmospheric equilibrium. Shaded region represents 1σ uncertainty. **D-F:** Carbon isotope fractionations defined in Fig.3.

called the vital effect. The magnitude of the vital effect increases with an increase in τ, but the direction of the vital effect depends on the ratio of the rates of calcification to photosynthetic carbon fixation ($R_{cal} : R_{fix}$) of the cell (Hermoso et al., 2016; McClelland et al., 2017). Carbon that leaks from the cell is depleted in ^{13}C relative to the intracellular pool, as the membrane is more permeable to the most ^{13}C-depleted phase of DIC, CO_2, than to HCO_3^-, which is ^{13}C-enriched. As τ increases, this leakage flux decreases, and the DIC pool in the cell becomes depleted in ^{13}C. This effect is most pronounced in cells with a relatively high $R_{cal} : R_{fix}$ ($\gtrsim 1$). In cells that have a low $R_{cal} : R_{fix}$ ($\lesssim 1$), the ^{13}C of the intracellular DIC pool is overprinted by leakage of ^{13}C-enriched carbon from the chloroplast. This interplay is affected by cellular compartmentation and intracellular bicarbonate transport (McClelland et al., 2017; Holtz et al., 2017). Although the large and variable nature of vital effects in coccolith calcite was once considered to be a negative attribute, which limited their utility in paleoclimate research, carbon isotope vital effects are themselves emerging as useful proxies, based on the observation that the difference in vital effects between taxa is reduced when τ is low (Bolton et al., 2012; Bolton and Stoll, 2013; Hermoso et al., 2020; Claxton et al., 2022).

Together, the carbon isotopes of coccolith calcite from the small and large size fractions ($\delta_{cal:S}$ and $\delta_{cal:L}$ respectively), and CAPs extracted from within ($\delta_{CAP:S}$ and $\delta_{CAP:L}$), in theory provide simultaneous constraints on the isotopic system independent of an external calcite reference, and with three degrees of freedom. However, given the large uncertainties in $\delta_{CAP:L}$, we consider just $\Delta_{cal:S\text{-}cal:L}$ and $\Delta_{cal:S\text{-}CAP:S}$.

4.1.1. *Response of $\Delta_{cal:S\text{-}cal:L}$*

The genus that dominates the small size fraction in this study (*Gephyrocapsa* spp.; 2-3 μm) has been shown in laboratory experiments to have a $R_{cal} : R_{fix}$ ratio of close to 1. Therefore, the magnitude of carbon isotopic vital effects in this size fraction is likely to be small. The large size fraction by contrast is dominated by *Coccolithus pelagicus* which has been shown to generally have a $R_{cal} : R_{fix}$ of > 1, thus the calcite that it produces is relatively ^{13}C-depleted, and this depletion is predicted to increase with increasing τ. Our data support these expectations, with $\delta_{cal:L}$ values being on average a couple of ‰ lower than $\delta_{cal:S}$ values, and each size fraction plotting either side of the planktic foraminifera record from this site, which is expected to exhibit small and relatively invariant vital effects. In time series, $\Delta_{cal:S\text{-}cal:L}$ decreases with increasing $[CO_2(aq)]$ over the highly resolved period of the glacial termination, as expected (Fig. 4 C and F). However, the lowest values of $\Delta_{cal:S\text{-}cal:L}$ occur early in the time series when pCO_2 is low. The increase in $\Delta_{cal:S\text{-}cal:L}$ between 190 and 160 ka that does not accompany a change in pCO_2 could have been driven by a shift in species composition within either the large or small size fractions. In the large size fraction this trend could be explained by an increasing fraction of forms with high $R_{cal} : R_{fix}$, or in the small size fraction by an increasing fraction of coccoliths from species with a low $R_{cal} : R_{fix}$. However we do not have quantitative species abundances for these samples which is required to decouple these

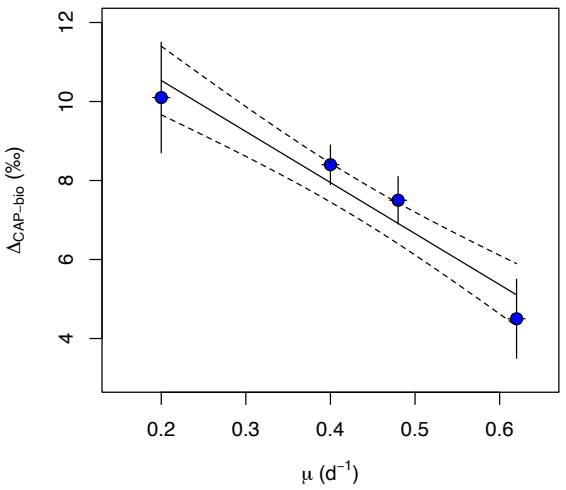

Figure 5: **Fractionation of carbon isotopes between CAPs and bulk biomass ($\epsilon_{CAP\text{-}bio}$).** A re-interpretation of the data of Wilkes et al. (2018). Here we hypothesise that changes in $\epsilon_{CAP\text{-}bio}$ are determined by growth rate alone. Equation of this OLS regression line is given in Eq.8.

possibilities (e.g. as in Claxton et al. (2022)).

4.2. Response of $\Delta_{cal:S\text{-}CAP:S}$

$\Delta_{cal:S\text{-}CAP:S}$ is dependent on processes affecting carbon isotope ratios of both the calcite and the CAPs (Fig.2). Absolute variation in $\delta_{cal:S}$ is relatively small over the glacial termination, but does change in such a way to dampen changes in $\Delta_{cal:S\text{-}CAP:S}$. For rough initial interpretations, we therefore assume a constant offset: $\Delta_{cal\text{-}DIC} = +1‰$. Over pH changes throughout a glacial cycle on the order of 0.2 pH units (Chalk et al., 2019), changes in DIC speciation have only a small effect on the fractionation of carbon isotopes between CO_2 and DIC (Zeebe and Wolf-Gladrow, 2001). Similarly, for an increase in temperature from ~11°C to ~17°C as inferred across the glacial termination, CO_2(aq) becomes less depleted relative to DIC by around 1‰. Like the coccolith calcite vital effects, these changes in SST and pH would have had the effect of dampening the change in $\Delta_{cal:S\text{-}CAP:S}$ across the glacial termination, and thus do not contribute to explaining the observed change in $\Delta_{cal:S\text{-}CAP:S}$. For simplicity, we therefore assume a constant offset: $\Delta_{DIC\text{-}CO_2} = +9$ ‰. $\Delta_{cal:S\text{-}CAP:S}$ is then roughly approximated by the following:

$$\Delta_{cal:S\text{-}CAP:S} \approx (\delta_{DIC} + 1‰) - \left(\delta_{DIC} - 9‰ - \epsilon_p + \epsilon_{CAP\text{-}bio}\right) \quad (6)$$

$$\approx 10‰ + \epsilon_p - \epsilon_{CAP\text{-}bio} \quad (7)$$

where $\epsilon_{CAP\text{-}bio}$ describes the fractionation of isotopes between CAPs and biomass. Given these assumptions, the observed change in $\Delta_{cal:S\text{-}CAP:S}$ over time therefore reflects a change in ϵ_p and / or $\epsilon_{CAP\text{-}bio}$.

Across the glacial termination, we would predict that the increase in CO_2 would drive an increase in ϵ_p, however, the $\Delta_{cal:S\text{-}CAP:S}$ curve is misaligned with that of the calculated history of [CO_2(aq)] at this site. Increases in temperature would likely cause an increase in average growth rate, and therefore drive a decrease in ϵ_p. However, the changes in temperature, which are well aligned with $\Delta_{cal:S\text{-}CAP:S}$ would drive ϵ_p in the wrong direction to explain the observed trend. We therefore explore how changes in the remaining variable in Eq. 7, $\epsilon_{CAP\text{-}bio}$, could be responsible for these signals.

4.3. Large vs. small CAP signals

While the uncertainties in $\delta_{CAP:L}$ values are too large for detailed interpretation, a surprising aspect of our dataset is that they are consistently more negative than $\delta_{CAP:S}$ values. According to Eq.5, larger cells are generally characterized by higher τ values, and therefore smaller ϵ_p, which corresponds to higher δ_{bio} values. One possibility that we have considered elsewhere is that larger cells may grow disproportionately slowly in the ocean owing to diffusion limitation of nutrients to the cell's surface (Pasciak and Gavis, 1974). Extremely slow nutrient-limited growth rates would also explain the flatter response of the large size fraction δ_{CAP} values to changes in temperature. This difference could alternatively be explained by a larger isotope effect imparted by the RuBisCO (ϵ_f) of coccolithophore species represented in the large size fraction. However, these measurements have not yet been made *in vitro* for large coccolithophores, and therefore, in the absence of evidence we assume that ϵ_f is constant. Lastly, this difference could also be achieved with similar δ_{bio} values in the large and small size fractions, but smaller values of $\epsilon_{CAP\text{-}bio}$ in the large size fraction. Wilkes et al. (2018) suggested that the variation in $\epsilon_{CAP\text{-}bio}$, and the constancy of $\epsilon_{alk\text{-}bio}$, in chemostat cultures is consistent with a constant partitioning of carbon between the broad classes of organic compounds, lipids, proteins and carbohydrates, but a variable partitioning of carbohydrate carbon between CAPs and other saccharides across experiments. However, it is unlikely that this constant partitioning between the broad classes holds when comparing taxa of highly contrasting cell size. Larger cells with lower surface area to volume ratios, will likely maintain a lower fraction of total fixed carbon as lipids (Finkel et al., 2016; Roy, 2018). Lipids are ^{13}C-depleted relative to bulk biomass, while carbohydrates are ^{13}C-enriched relative to bulk biomass. For a larger cell with a lower lipid fraction, the isotopic partitioning between the broad classes of lipids and carbohydrates would shift, resulting in large cells with ^{13}C-depleted lipids and ^{13}C-depleted carbohydrates (including CAPs) relative to smaller cells (Hayes, 2002).

4.4. Reconciling alkenones and CAPs

The alkenone CO_2 proxy has been calibrated with culture experiments (Popp et al., 1998), and shown to vary as predicted with seawater CO_2 concentrations in the modern ocean (Pagani et al., 2002; Pagani, 2002). However, drill core studies using alkenones as the sedimentary organic matter target have shown that δ_{alk} is often relatively invariant over glacial/interglacial cycles despite large changes in [CO_2(aq)] (Zhang et al., 2013; Badger et al., 2019; Badger, 2021). Alkenone carbon isotope

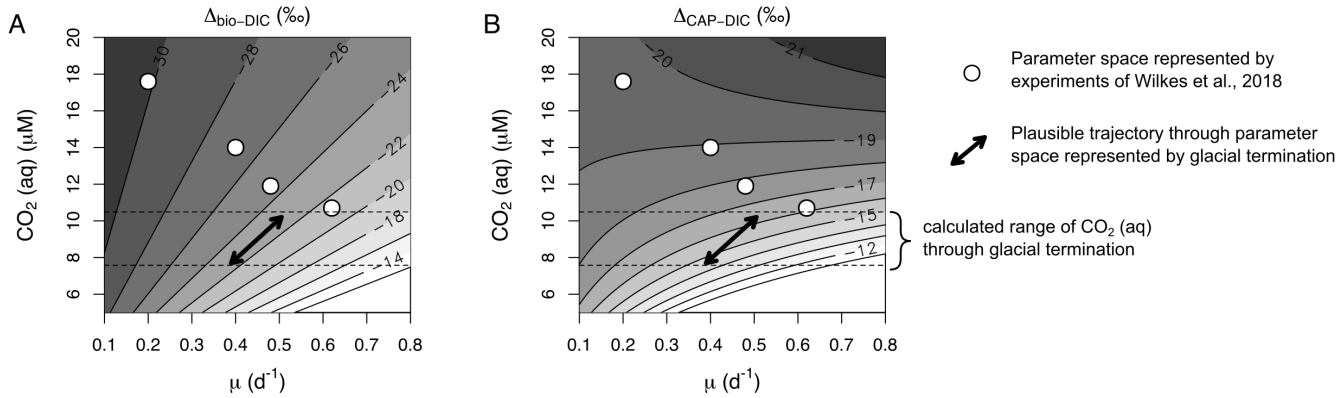

Figure 6: **Isotope fractionation in a CO_2 and growth rate (μ) parameter space. A)** $\Delta_{\text{bio-DIC}}$ as a function of CO_2 and μ. Contours are calculated according to the following equation: $\Delta_{\text{bio-DIC}} = 189.8\frac{\mu}{CO_2} - 32.3$ (assuming a constant δ_{DIC} between experiments of Wilkes et al. (2018)). **B)** $\Delta_{\text{CAP-DIC}}$ as a function of CO_2 and μ. Equation used to generate contours is given by: $\Delta_{\text{CAP-DIC}} = \Delta_{\text{bio-DIC}} + \Delta_{\text{CAP-bio}}$. $\Delta_{\text{CAP-bio}}$ as a function of μ is given in the text (Eq. 8). In both panels, white points represent the parameter space represented by chemostat data from (Wilkes et al., 2018). Across the four experiments represented by these points, a greater range of values are seen in $\Delta_{\text{bio-DIC}}$ than in $\Delta_{\text{CAP-DIC}}$. The dashed lines represent the approximate range of glacial-interglacial [CO_2 (aq)]. In both panels, the black arrow represents the same possible path in parameter space within this CO_2 change where a slight increase in μ results in negligible change in $\Delta_{\text{bio-DIC}}$, but a significant change in $\Delta_{\text{CAP-DIC}}$.

values (δ_{alk}) are consistently around 4 ‰ lower than δ_{bio} across a wide range of conditions (i.e. $\delta_{\text{bio}} = \delta_{\text{alk}} + 4$ ‰) (Schouten et al., 1998; Laws et al., 2001; Wilkes et al., 2017) (Fig. 2; however, it should be noted that this relationship has been established only for the relatively recent species, *G. huxleyi*). As alkenones exhibit a constant isotopic offset from biomass, explanations for this apparent insensitivity have focused on mechanisms that could counter the effect of changes in CO_2 on bulk biomass. One possibility is that changes in growth rate parallel the change in CO_2 (Badger et al., 2019; Zhang et al., 2020). As μ and C_e appear on opposite sides of the ratio in Eq. 5, an increase in μ with increasing C_e could minimize changes in τ. A second possibility is an increase in the uptake of carbon during periods of low C_e (Stoll et al., 2019; Badger, 2021). As K and C_e appear on the same side of the ratio in Eq. 5, an increase in K when C_e is low would also minimize the impact on τ. Both mechanisms make sense physiologically, however, neither explain the changes we observe in $\Delta_{\text{cal-CAP}}$.

We present a hypothesis that is consistent with an insensitivity of ϵ_p to changes associated with glacial cycles, and therefore involves changes in $\epsilon_{\text{CAP-bio}}$. Wilkes et al. (2018) showed that CAPs are enriched in ^{13}C relative to bulk biomass, and that this enrichment decreases with increasing μ/CO_2 ($\propto \tau$ at constant r). In these experiments, the variables μ and CO_2 were not decoupled (white points, Fig. 6 show the parameter space explored), and results were originally interpreted relative to the compound variable, μ/CO_2. Here we hypothesise that $\epsilon_{\text{CAP-bio}}$ in the experiments of Wilkes et al. (2018) is driven by changes in μ, and is independent of CO_2. A linear regression between $\epsilon_{\text{CAP-bio}}$ and μ from the experiments of Wilkes et al. (2018) (Fig. 5) gives the following equation:

$$\epsilon_{\text{CAP-bio}} = 13.1 - 12.9\mu. \quad (8)$$

Under this interpretation, while $\Delta_{\text{bio-DIC}}$ is a function of μ/CO_2 (straight contours in Fig. 6A), $\Delta_{\text{CAP-DIC}}$ is a combined function of both μ/CO_2 and μ (curved contours in Fig. 6B). We conclude that coupled increases in μ and CO_2 could theoretically result in no changes in $\Delta_{\text{bio-DIC}}$, and therefore no changes in $\Delta_{\text{alk-DIC}}$ (i.e. black arrow does not cross contours in Fig. 6A), but drive an increase in the magnitude of $\Delta_{\text{CAP-DIC}}$ (i.e. black arrow does cross contours in Fig. 6B).

The positive effect of temperature on μ in the species present in our samples (over low to moderate temperatures) is well established (e.g. Buitenhuis et al., 2008; Sett et al., 2014). Therefore, while instantaneous growth rate in the surface ocean above our core location was probably limited by nutrient concentrations or light availability, the inferred ~6°C SST increase that accompanied the deglaciation at this site would likely have induced an increase in average μ during times of exponential growth. In our data, we find a strong correlation between $\Delta_{\text{cal-CAP}}$ and reconstructed SSTs (Fig. 7), which supports this hypothesis.

5. Conclusions

Coccolith associated polysaccharides (CAPs) are a promising new target for organic matter analysis in sediments, which may reveal insights into metabolic rates of ancient algae. We have shown that pristine CAPs can be successfully extracted from within calcite fossil coccoliths from marine sediments, purified and isotopically analysed. The carbon isotope ratios of these molecules appear to be primarily controlled by temperature regulated growth rate changes, but further experimental investigation is required before its use as a quantitative proxy can be realized. Specifically, it will be necessary to better understand the biochemistry of CAP formation in calcifying algae, and the isotope effects associated with each biosynthetic step. It will be furthermore essential to determine how organic carbon and carbon isotope partitioning differs between species, and between cells of different sizes. The ubiquity and

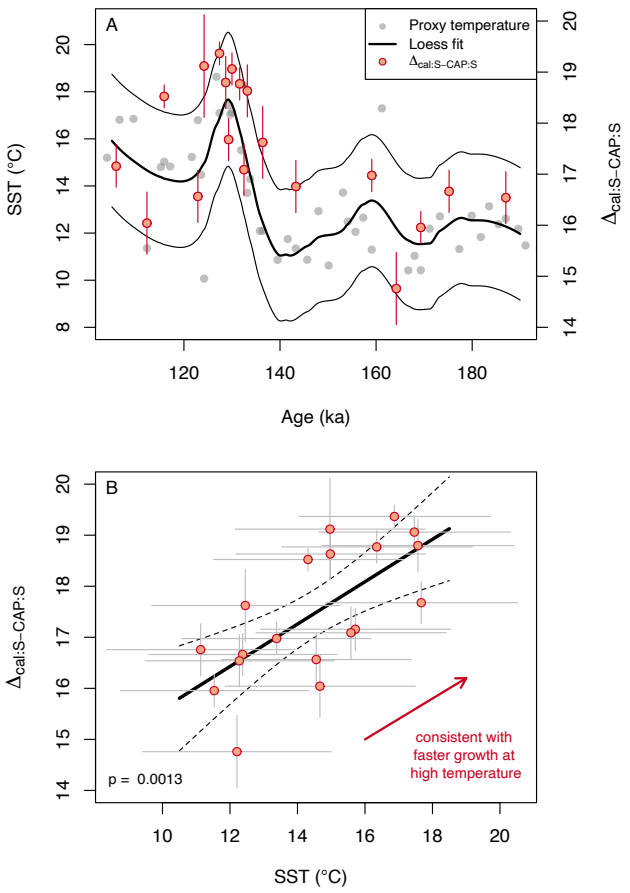

Figure 7: **Hypothesis: Temperature-controlled changes in growth rate dominate changes in $\Delta_{\text{CAP-cal}}$.** **A:** U^{k}_{37}, SST record plotted underneath $\Delta_{\text{CAP-cal}}$ data against time. **B:** $\Delta_{\text{CAP-cal}}$ for each sample plotted directly against interpolated LOESS fit to U^{k}_{37}, SST.

high preservation of CAPs extends the species-specific organic matter record back over 200 million years into the geologic past, and, with sufficient material, opens up the possibility of species-specific records of organic carbon across multiple sizes of coccolithophore simultaneously. The unambiguous association between the organic carbon isotope measurement and fossils of the host organism will be invaluable. As with the modest original applications of ϵ_p (Freeman and Hayes, 1992), precise interpretations of $\Delta_{\text{cal-CAP}}$ from sediments will likely be elusive. However, approaches using CAPs as the target for organic geochemical analysis have the potential to constrain parameter space more comprehensively than has previously been possible, and extend investigations of CO_2 and algal physiology 200 million years to the Late Triassic.

6. Data

The new data (temperature and isotope data) contained in the manuscript are available through the UCL Research Data Repository with DOI:10.5522/04/25251685 (https://doi.org/10.5522/04/25251685.v1).

7. CRediT authorship

HM: Conceptualization, Formal analysis, Investigation, Writing - Original Draft, Visualization, **RL:** Conceptualization, Methodology, Writing - Review & Editing, Supervision, **AP:** Methodology, Investigation, Resources, Writing - Review & Editing, **RR:** Conceptualization, Resources, Writing - Review & Editing, Supervision, Funding acquisition.

8. Acknowledgements

This work was undertaken as part of UKRI projects, NE/H017119/1 and NE/V011049/1. Thanks to Michaël Hermoso for sharing microfiltration expertise, Caroline Anderson for early conceptual discussions, Despoina Mavridou for laboratory assistance, and Elise Wilkes for helpful discussions. A.P. acknowledges funding from the Gordon and Betty Moore Foundation and NSF award 2100509, and thanks Pratigya Polissar and Sam Phelps for helpful discussions.

9. Appendix A. Supplementary Material

A supplementary figure is provided comparing the temperature records derived using the $U^{k'}_{37}$ and TEX_{86} proxies, and their relationships to $\Delta_{\text{cal-CAP}}$.

References

Andruleit, H., Rogalla, U., Stäger, S., 2004. From living communities to fossil assemblages: Origin and fate of coccolithophores in the northern Arabian Sea. Micropaleontology 50, 5–21. doi:10.2113/50.Suppl{_}1.5.

Arthur, M.A., Dean, W.E., Claypool, G.E., 1985. Anomalous ^{13}C enrichment in modern marine organic carbon. Nature 315, 216–218. doi:10.1038/315216a0.

Badger, M.P., Chalk, T.B., Foster, G.L., Bown, P.R., Gibbs, S.J., Sexton, P.F., Schmidt, D.N., Pälike, H., Mackensen, A., Pancost, R.D., 2019. Insensitivity of alkenone carbon isotopes to atmospheric CO_2 at low to moderate CO_2 levels. Climate of the Past 15, 539–554. doi:10.5194/cp-15-539-2019.

Badger, M.P., Lear, C.H., Pancost, R.D., Foster, G.L., Bailey, T.R., Leng, M.J., Abels, H.A., 2013. CO_2 drawdown following the middle Miocene expansion of the Antarctic Ice Sheet. Paleoceanography 28, 42–53. doi:10.1002/palo.20015.

Badger, M.P., 2021. Alkenone isotopes show evidence of active carbon concentrating mechanisms in coccolithophores as aqueous carbon dioxide concentrations fall below 7 mmol. Biogeosciences 18, 1149–1160. doi:10.5194/bg-18-1149-2021.

Bazin, L., Landais, A., Lemieux-Dudon, B., Toyé Mahamadou Kele, H., Veres, D., Parrenin, F., Martinerie, P., Ritz, C., Capron, E., Lipenkov, V., Loutre, M.F., Raynaud, D., Vinther, B., Svensson, A., Rasmussen, S.O., Severi, M., Blunier, T., Leuenberger, M., Fischer, H., Masson-Delmotte, V., Chappellaz, J., Wolff, E., 2013. An optimized multi-proxy, multi-site Antarctic ice and gas orbital chronology (AICC2012): 120–800 ka. Climate of the Past 9, 1715–1731. doi:10.5194/cp-9-1715-2013.

Becker, K.W., Lipp, J.S., Versteegh, G.J., Wörmer, L., Hinrichs, K.U., 2015. Rapid and simultaneous analysis of three molecular sea surface temperature proxies and application to sediments from the Sea of Marmara. Organic Geochemistry 85, 42–53. doi:10.1016/j.orggeochem.2015.04.008.

Bereiter, B., Eggleston, S., Schmitt, J., Nehrbass-Ahles, C., Stocker, T.F., Fischer, H., Kipfstuhl, S., Chappellaz, J., 2015. Revision of the EPICA Dome C CO_2 record from 800 to 600-kyr before present. Geophysical Research Letters 42, 542–549. doi:10.1002/2014GL061957.

Bidigare, R.R., Fluegge, A., Freeman, K.H., Hanson, K.L., Hayes, J.M., Hollander, D., Jasper, J.P., King, L.L., Laws, E.A., Milder, J., Millero, F.J., Pancost, R., Popp, B.N., Steinberg, P.A., Wakeham, S.G., 1997. Consistent fractionation of ^{13}C in nature and in the laboratory: Growth-rate effects in some haptophyte algae. Global Biogeochemical Cycles 11, 279–292. doi:10.1029/96GB03939.

Boller, A.J., Thomas, P.J., Cavanaugh, C.M., Scott, K.M., 2011. Low stable carbon isotope fractionation by coccolithophore RubisCO. Geochimica et Cosmochimica Acta 75, 7200–7207. doi:10.1016/j.gca.2011.08.031.

Boller, A.J., Thomas, P.J., Cavanaugh, C.M., Scott, K.M., 2015. Isotopic discrimination and kinetic parameters of RubisCO from the marine bloom-forming diatom, Skeletonema costatum. Geobiology 13, 33–43. doi:10.1111/gbi.12112.

Bolton, C.T., Hernandez-Sanchez, M., Fuertes, M.A., Gonzalez-Lemos, S., Abrevaya, L., Mendez-Vicente, A., Flores, J.A., Probert, I., Giosan, L., Johnson, J., Stoll, H.M., 2016. Decrease in coccolithophore calcification and CO_2 since the middle Miocene. Nature Communications 7. doi:10.1038/ncomms10284.

Bolton, C.T., Stoll, H.M., 2013. Late Miocene threshold response of marine algae to carbon dioxide limitation. Nature 500, 558–562. URL: http://dx.doi.org/10.1038/nature12448, doi:10.1038/nature12448.

Bolton, C.T., Stoll, H.M., Mendez-Vicente, A., 2012. Vital effects in coccolith calcite: Cenozoic climate pCO_2 drove the diversity of carbon acquisition strategies in coccolithophores? Paleoceanography 27, 1–16. doi:10.1029/2012PA002339.

Brassell, S.C., Dumitrescu, M., Bralower, T.J., Premoli-Silva, I., Malone, M.J., Arthur, M.A., Averyt, K., Bown, P., Channell, J.E., Clarke, L.J., Dutton, A.L., Eleson, J.W., Frank, T.D., Gylesjö, S., Hancock, H., Kano, H., Leckie, R.M., Marsaglia, K.M., McGuire, J., Moe, K.T., Petrizzo, M.R., Robinson, S., Röhl, U., Sager, W.W., Takeda, K., Thomas, D., Williams, T., Zachos, J.C., 2004. Recognition of alkenones in a lower Aptian porcellanite from the west-central Pacific. Organic Geochemistry 35, 181–188. doi:10.1016/j.orggeochem.2003.09.003.

Buitenhuis, E.T., Pangerc, T., Franklin, D.J., Quéré, C.L., Malin, G., 2008. Growth rates of six coccolithophorid strains as a function of temperature. Limnology and Oceanography 53, 1181–1185. doi:10.4319/lo.2008.53.3.1181.

Cassar, N., Laws, E.A., Popp, B.N., 2006. Carbon isotopic fractionation by the marine diatom Phaeodactylum tricornutum under nutrient- and light-limited growth conditions. Geochimica et Cosmochimica Acta 70, 5323–5335. doi:10.1016/j.gca.2006.08.024.

Chalk, T., Foster, G., Wilson, P., 2019. Dynamic storage of glacial CO_2 in the Atlantic Ocean revealed by boron and pH records. Earth and Planetary Science Letters 510, 1–11. doi:10.1016/j.epsl.2018.12.022.

Claxton, L.M., McClelland, H.L.O., Hermoso, M., Rickaby, R.E.M., 2022. Eocene emergence of highly calcifying coccolithophores despite declining atmospheric CO_2. Nature Geoscience 15, 826–831. doi:10.1038/s41561-022-01006-0.

Conte, M.H., Thompson, A., Eglinton, G., Green, J.C., 1995. Lipid Biomarker Diversity in the Coccolithophorid Emiliania huxleyi (Prymnesiophyceae) and the Related Species Gephyrocapsa oceanica. Journal of Phycology 31, 272–282. doi:10.1111/j.0022-3646.1995.00272.x.

De Jong, E.W., Bosch, L., Westbroek, P., 1976. Isolation and Characterization of a Ca^{2+} Binding Polysaccharide Associated with Coccoliths of Emiliania huxleyi (Lohmann) Kamptner. European Journal of Biochemistry 70, 611–621. doi:10.1111/j.1432-1033.1976.tb11052.x.

Dean, W.E., Arthur, M.A., Claypool, G.E., 1986. Depletion of ^{13}C in Cretaceous marine organic matter: Source, diagenetic, or environmental signal? Marine Geology 70, 119–157. doi:10.1016/0025-3227(86)90092-7.

Elderfield, H., Ferretti, P., Greaves, M., Crowhurst, S., McCave, I.N., Hodell, D., Piotrowski, A.M., 2012a. Evolution of ocean temperature and ice volume through the mid-Pleistocene climate transition. Science 337, 704–709. doi:10.1126/science.1221294.

Elderfield, H., Ferretti, P., Greaves, M., Crowhurst, S.J., McCave, I.N., Hodell, D.a., Piotrowski, A.M., 2012b. Evolution of ocean temperature. Science 337, 704–709. doi:10.1594/PANGAEA.786205.

Falkowski, P.G., 1991. Species variability in the fractionation of ^{13}C and ^{12}C by marine phytoplankton. Journal of Plankton Research 13, 21–28. doi:10.1093/oxfordjournals.plankt.a042367.

Farquhar, G.D., O'Leary, M.H., Berry, J.A., 1982. On the relationship between carbon isotope discrimination and the intercellular carbon dioxide concentration in leaves. Australian Journal of Plant Physiology 9, 121–137. doi:10.1071/PP9820121.

Finkel, Z.V., Follows, M.J., Irwin, A.J., 2016. Size-scaling of macromolecules and chemical energy content in the eukaryotic microalgae. Journal of Plankton Research 38, 1151–1162. doi:10.1093/plankt/fbw057.

Freeman, K.H., Hayes, J.M., 1992. Fractionation of carbon isotopes by phytoplankton and estimates of ancient CO_2 levels. Global Biogeochemical Cycles 6, 185–198. doi:10.1029/92GB00190.

Freudenthal, T., Wagner, T., Wenzhöfer, F., Zabel, M., Wefer, G., 2001. Early diagenesis of organic matter from sediments of the Eastern subtropical Atlantic: Evidence from stable nitrogen and carbon isotopes. Geochimica et Cosmochimica Acta 65, 1795–1808. doi:10.1016/S0016-7037(01)00554-3.

Gattuso, J.P., Epitalon, J.M., Lavigne, H., 2022. Seacarb: Seawater Carbonate Chemistry R package version 3.3.1. URL: https://cran.r-project.org/package=seacarb.

Gould, S.B., Waller, R.F., McFadden, G.I., 2008. Plastid Evolution. Annual Review of Plant Biology 59, 491–517. doi:10.1146/annurev.arplant.59.032607.092915.

Hayes, J.M., 1993. Factors controlling ^{13}C contents of sedimentary organic compounds: Principles and evidence. Marine Geology 113, 111–125. doi:10.1016/0025-3227(93)90153-M.

Hayes, J.M., 2002. Practice and Principles of Isotopic Measurements in Organic Geochemistry. Society .

Hayes, J.M., Strauss, H., Kaufman, A.J., 1999. The abundance of ^{13}C in marine organic matter and isotopic fractionation in the global biogeochemical cycle of carbon during the past 800 Ma. Chemical Geology 161, 103–125. doi:10.1016/S0009-2541(99)00083-2.

Hayes, J.M., Takigiku, R., Ocampo, R., Callot, H.J., Albrecht, P., 1987. Isotopic compositions and probable origins of organic molecules in the Eocene Messel shale. Nature 329, 48–51. doi:10.1038/329048a0.

Hayes, J.M., Waldbauer, J.R., 2006. The carbon cycle and associated redox processes through time. Philosophical Transactions of the Royal Society B: Biological Sciences 361, 931–950. doi:10.1098/rstb.2006.1840.

Henderiks, J., 2008. Coccolithophore size rules - Reconstructing ancient cell geometry and cellular calcite quota from fossil coccoliths. Marine Micropaleontology 67, 143–154. doi:10.1016/j.marmicro.2008.01.005.

Henderiks, J., Pagani, M., 2008. Coccolithophore cell size and the Paleogene decline in atmospheric CO_2. Earth and Planetary Science Letters 269, 576–584. doi:10.1016/j.epsl.2008.03.016.

Henderiks, J., Rickaby, R.E., 2007. A coccolithophore concept for constraining the Cenozoic carbon cycle. Biogeosciences 4, 323–329. doi:10.5194/bg-4-323-2007.

Herfort, L., Thake, B., Roberts, J., 2002. Acquisition and use of bicarbonate by Emiliania huxleyi. New Phytologist 156, 427–436. doi:10.1046/j.1469-8137.2002.00523.x.

Hermoso, M., McClelland, H.L.O., Hirst, J.S., Minoletti, F., Bonifacie, M., Rickaby, R.E., 2020. Towards the use of the coccolith vital effects in palaeoceanography: A field investigation during the middle Miocene in the SW Pacific Ocean. Deep-Sea Research Part I: Oceanographic Research Papers doi:10.1016/j.dsr.2020.103262.

Hermoso, M., Minoletti, F., Aloisi, G., Bonifacie, M., McClelland, H.L., Labourdette, N., Renforth, P., Chaduteau, C., Rickaby, R.E., 2016. An explanation for the ^{18}O excess in Noelaerhabdaceae coccolith calcite. Geochimica et Cosmochimica Acta 189, 132–142. doi:10.1016/j.gca.2016.06.016.

Hollander, D.J., McKenzie, J.A., 1991. CO_2 control on carbon-isotope fractionation during aqueous photosynthesis: a paleo-pCO_2 barometer. Geology 19, 929–932. doi:10.1130/0091-7613(1991)019<0929:CCOCIF>2.3.CO;2.

Holtz, L.M., Wolf-Gladrow, D., Thoms, S., 2017. Stable carbon isotope signals in particulate organic and inorganic carbon of coccolithophores – A numerical model study for Emiliania huxleyi. Journal of Theoretical Biology 420, 117–127. doi:10.1016/j.jtbi.2017.01.030.

Hurley, S.J., Wing, B.A., Jasper, C.E., Hill, N.C., Cameron, J.C., 2021. Carbon isotope evidence for the global physiology of Proterozoic cyanobacteria. Science Advances 7, 1–9. doi:10.1126/sciadv.abc8998.

Jasper, J.P., Hayes, J.M., 1990. A carbon isotope record of CO_2 levels during the late Quaternary. Nature 347, 462–464. doi:10.1038/347462a0.

Jasper, J.P., Hayes, J.M., Mix, A.C., Prahl, F.G., 1994. Photosynthetic fractionation of ^{13}C and concentrations of dissolved CO_2 in the central equatorial Pacific during the last 255,000 years. Paleoceanography 9, 781–798. doi:10.1029/94PA02116.

Karhu, J.A., Holland, H.D., 1996. Carbon isotopes and the rise of atmospheric oxygen. Geology 24, 867–870. doi:10.1130/0091-7613(1996)024<0867:CIATRO>2.3.CO;2.

Keller, K., Morel, F.M., 1999. A model of carbon isotopic fractionation and active carbon uptake in phytoplankton. Marine Ecology Progress Series 182, 295–298. doi:10.3354/meps182295.

Kottmeier, D.M., Rokitta, S.D., Tortell, P.D., Rost, B., 2014. Strong shift from HCO_3^- To CO_2 uptake in Emiliania huxleyi with acidification: New approach unravels acclimation versus short-term pH effects. Photosynthesis Research 121, 265–275. doi:10.1007/s11120-014-9984-9.

Langer, G., Gussone, N., Nehrke, G., Riebesell, U., Eisenhauer, A., Kuhnert, H., Rost, B., Trimborn, S., Thoms, S., 2006. Coccolith strontium to calcium ratios in Emiliania huxleyi: The dependence on seawater strontium and calcium concentrations. Limnology and Oceanography 51, 310–320. doi:10.4319/lo.2006.51.1.0310.

Laws, E.A., Popp, B.N., Bidigare, R.R., Kennicutt, M.C., Macko, S.A., 1995. Dependence of phytoplankton carbon isotopic composition on growth rate and $[CO_2)aq$: Theoretical considerations and experimental results. Geochimica et Cosmochimica Acta 59, 1131–1138. doi:10.1016/0016-7037(95)00030-4.

Laws, E.A., Popp, B.N., Bidigare, R.R., Riebesell, U., Burkhardt, S., Wakeham, S.G., 2001. Controls on the molecular distribution and carbon isotopic composition of alkenones in certain haptophyte algae. Geochemistry, Geophysics, Geosystems 2, 2000GC000057. doi:10.1029/2000gc000057.

Laws, E.A., Popp, B.N., Cassar, N., Tanimoto, J., 2002. ^{13}C discrimination patterns in oceanic phytoplankton: Likely influence of CO_2 concentrating mechanisms, and implications for palaeoreconstructions. Functional Plant Biology 29, 323–333. doi:10.1071/pp01183.

Lee, R.B., Mavridou, D.A., Papadakos, G., McClelland, H.L., Rickaby, R.E., 2016. The uronic acid content of coccolith-associated polysaccharides provides insight into coccolithogenesis and past climate. Nature Communications 7, 1–7. doi:10.1038/ncomms13144.

Lisiecki, L.E., Raymo, M.E., 2005. A Pliocene-Pleistocene stack of 57 globally distributed benthic $\delta\ ^{18}O$ records. Paleoceanography 20, 1–17. doi:10.1029/2004PA001071.

Liu, H., Aris-Brosou, S., Probert, I., De Vargas, C., 2010. A time line of the environmental genetics of the haptophytes. Molecular Biology and Evolution 27, 161–176. doi:10.1093/molbev/msp222.

Marlowe, I.T., Brassell, S.C., Eglinton, G., Green, J.C., 1990. Long-chain alkenones and alkyl alkenoates and the fossil coccolith record of marine sediments. Chemical Geology 88, 349–375. doi:10.1016/0009-2541(90)90098-R.

Marsh, M.E., 1994. Polyanion-mediated mineralization - assembly and reorganization of acidic polysaccharides in the Golgi system of a coccolithophorid alga during mineral deposition. Protoplasma 177, 108–122. doi:10.1007/BF01378985.

Marsh, M.E., Chang, D.K., King, G.C., 1992. Isolation and characterization of a novel acidic polysaccharide containing tartrate and glyoxylate residues from the mineralized scales of a unicellular coccolithophorid alga Pleurochrysis carterae. Journal of Biological Chemistry 267, 20507–20512.

Marsh, M.E., Ridall, A.L., Azadi, P., Duke, P.J., 2002. Galacturonomannan and Golgi-derived membrane linked to growth and shaping of biogenic calcite. Journal of Structural Biology 139, 39–45. doi:10.1016/S1047-8477(02)00503-8.

Martínez-Botí, M.A., Foster, G.L., Chalk, T.B., Rohling, E.J., Sexton, P.F., Lunt, D.J., Pancost, R.D., Badger, M.P., Schmidt, D.N., 2015. Plio-Pleistocene climate sensitivity evaluated using high-resolution CO_2 records. Nature 518, 49–54. doi:10.1038/nature14145.

McClelland, H.L., Barbarin, N., Beaufort, L., Hermoso, M., Ferretti, P., Greaves, M., Rickaby, R.E., 2016. Calcification response of a key phytoplankton family to millennial-scale environmental change. Scientific Reports 6, 1–11. doi:10.1038/srep34263.

McClelland, H.L., Bruggeman, J., Hermoso, M., Rickaby, R.E., 2017. The origin of carbon isotope vital effects in coccolith calcite. Nature Communications 8, 1–16. doi:10.1038/ncomms14511.

Minoletti, F., Hermoso, M., Gressier, V., 2009. Separation of sedimentary micron-sized particles for palaeoceanography and calcareous nannoplankton biogeochemistry. Nature Protocols 4, 14–24. doi:10.1038/nprot.2008.200.

Mollenhauer, G., Eglinton, T., Ohkouchi, N., Schneider, R., Müller, P., Grootes, P., Rullkötter, J., 2003. Asynchronous alkenone and foraminifera records from the Benguela Upwelling System. Geochimica et Cosmochimica Acta 67, 2157–2171. doi:10.1016/S0016-7037(03)00168-6.

Müller, P.J., Kirst, G., Ruhland, G., Von Storch, I., Rosell-Melé, A., 1998. Calibration of the alkenone paleotemperature index U37K based on core-tops from the eastern South Atlantic and the global ocean (60°N-60°S). Geochimica et Cosmochimica Acta 62, 1757–1772. doi:10.1016/S0016-7037(98)00097-0.

Nimer, N.A., Iglesias-Rodriguez, M.D., Merrett, M.J., 1997. Bicarbonate utilization by marine phytoplankton species. Journal of Phycology 33, 625–631. doi:10.1111/j.0022-3646.1997.00625.x.

Nimer, N.A., Merrett, M.J., Brownlee, C., 1996. Inorganic carbon transport in relation to culture age and inorganic carbon concentration in a high-calcifying strain of Emiliania huxleyi (prymnesiophyceae). Journal of Phycology 32, 813–818. doi:10.1111/j.0022-3646.1996.00813.x.

Ohkouchi, N., Eglinton, T.I., Keigwin, L.D., Hayes, J.M., 2002. Spatial and temporal offsets between proxy records in a sediment drift. Science 298, 1224–1227. doi:10.1126/science.1075287.

Pagani, M., 2002. The alkenone - CO_2 proxy and ancient atmospheric carbon dioxide. Philosophical Transactions of the Royal Society A: Mathematical, Physical and Engineering Sciences 360, 609–632. doi:10.1098/rsta.2001.0959.

Pagani, M., Freeman, K.H., Arthur, M.A., 1999. Late miocene atmospheric CO_2 concentrations and the expansion of C4 grasses. Science 285, 876–879. doi:10.1126/science.285.5429.876.

Pagani, M., Freeman, K.H., Ohkouchi, N., Caldeira, K., 2002. Comparison of water column $[CO_2$ (aq)] with sedimentary alkenone-based estimates: A test of the alkenone-CO_2 proxy . Paleoceanography 17, 21–1. doi:10.1029/2002pa000756.

Pagani, M., Huber, M., Liu, Z., Bohaty, S.M., Henderiks, J., Sijp, W., Krishnan, S., DeConto, R.M., 2011. The role of carbon dioxide during the onset of antarctic glaciation. Science 334, 1261–1264. doi:10.1126/science.1203909.

Pagani, M., Lemarchand, D., Spivack, A., Gaillardet, J., 2005. A critical evaluation of the boron isotope-pH proxy: The accuracy of ancient ocean pH estimates. Geochimica et Cosmochimica Acta 69, 953–961. doi:10.1016/j.gca.2004.07.029.

Pasciak, W.J., Gavis, J., 1974. Transport limitation of nutrient uptake in phytoplankton. Limnology and Oceanography 19, 881–888. doi:10.4319/lo.1974.19.6.0881.

Pearson, A., 2010. Pathways of Carbon Assimilation and Their Impact on Organic Matter Values $\delta^{13}C$, in: Handbook of Hydrocarbon and Lipid Microbiology. Springer Berlin Heidelberg, Berlin, Heidelberg, pp. 143–156. doi:10.1007/978-3-540-77587-4{_}9.

Phelps, S.R., Stoll, H.M., Bolton, C.T., Beaufort, L., Polissar, P.J., 2021. Controls on Alkenone Carbon Isotope Fractionation in the Modern Ocean. Geochemistry, Geophysics, Geosystems 22. doi:10.1029/2021GC009658.

Polik, C.A., Elling, F.J., Pearson, A., 2018. Impacts of Paleoecology on the TEX_{86} Sea Surface Temperature Proxy in the Pliocene-Pleistocene Mediterranean Sea. Paleoceanography and Paleoclimatology 33, 1472–1489. doi:10.1029/2018PA003494.

Popp, B.N., Laws, E.A., Bidigare, R.R., Dore, J.E., Hanson, K.L., Wakeham, S.G., 1998. Effect of phytoplankton cell geometry on carbon isotopic fractionation. Geochimica et Cosmochimica Acta 62, 69–77. doi:10.1016/S0016-7037(97)00333-5.

Ramus, J., 1977. Alcian Blue: a Quantitative Aqueous Assay for Algal Acid and Sulfated Polysaccharides. doi:10.1111/j.1529-8817.1977.tb02939.x.

Rau, G.H., Froelich, P.N., Takahashi, T., Des Marais, D.J., 1991. Does Sedimentary Organic $\delta^{13}C$ Record Variations in Quaternary Ocean $[CO_2(aq)]$? Paleoceanography 6, 335–347. doi:10.1029/91PA00321.

Rau, G.H., Riebesell, U., Wolf-Gladrow, D., 1996. A model of photosynthetic ^{13}C fractionation by marine phytoplankton based on diffusive molecular CO_2 uptake. Marine Ecology Progress Series 133, 275–285. doi:10.3354/meps133275.

Rickaby, R.E.M., Schrag, D.P., Zondervan, I., Riebesell, U., 2002. Growth rate

dependence of Sr incorporation during calcification of Emiliania huxleyi . Global Biogeochemical Cycles 16, 6–1. doi:10.1029/2001gb001408.

Riebesell, U., Wolf-Gladrow, D.A., Smetacek, V., 1993. Carbon dioxide limitation of marine phytoplankton growth rates. Nature 361, 249–251. doi:10.1038/361249a0.

Rost, B., Zondervan, I., Riebesell, U., 2002. Light-dependent carbon isotope fractionation in the coccolithophorid Emiliania huxleyi. Limnology and Oceanography 47, 120–128. doi:10.4319/lo.2002.47.1.0120.

Roy, S., 2018. Distributions of phytoplankton carbohydrate, protein and lipid in the world oceans from satellite ocean colour. The ISME Journal 12, 1457–1472. doi:10.1038/s41396-018-0054-8.

Schouten, S., Hopmans, E.C., Schefuß, E., Sinninghe Damsté, J.S., 2002. Distributional variations in marine crenarchaeotal membrane lipids: a new tool for reconstructing ancient sea water temperatures? Earth and Planetary Science Letters 204, 265–274. doi:10.1016/S0012-821X(02)00979-2.

Schouten, S., Klein Breteler, W.C., Blokker, P., Schogt, N., Rijpstra, W.I.C., Grice, K., Baas, M., Sinninghe Damsté, J.S., 1998. Biosynthetic effects on the stable carbon isotopic compositions of algal lipids: implications for deciphering the carbon isotopic biomarker record. Geochimica et Cosmochimica Acta 62, 1397–1406. doi:10.1016/S0016-7037(98)00076-3.

Seki, O., Foster, G.L., Schmidt, D.N., Mackensen, A., Kawamura, K., Pancost, R.D., 2010. Alkenone and boron-based Pliocene pCO_2 records. Earth and Planetary Science Letters 292, 201–211. doi:10.1016/j.epsl.2010.01.037.

Sessions, A.L., Sylva, S.P., Hayes, J.M., 2005. Moving-wire device for carbon isotopic analyses of nanogram quantities of nonvolatile organic carbon. Analytical Chemistry 77, 6519–6527. doi:10.1021/ac051251z.

Sett, S., Bach, L.T., Schulz, K.G., Koch-Klavsen, S., Lebrato, M., Riebesell, U., 2014. Temperature modulates coccolithophorid sensitivity of growth, photosynthesis and calcification to increasing seawater pCO_2. PLoS ONE 9. doi:10.1371/journal.pone.0088308.

Sharkey, T.D., Berry, J.A., 1985. Carbon isotope fractionation of algae as influenced by an inducible CO_2 concentration mechanism. The American Society of Plant Physiologists , 389–401.

Stoll, H.M., Guitian, J., Hernandez-Almeida, I., Mejia, L.M., Phelps, S., Polissar, P., Rosenthal, Y., Zhang, H., Ziveri, P., 2019. Upregulation of phytoplankton carbon concentrating mechanisms during low CO_2 glacial periods and implications for the phytoplankton pCO_2 proxy. Quaternary Science Reviews 208, 1–20. doi:10.1016/j.quascirev.2019.01.012.

Stoll, H.M., Schrag, D.P., 2000. Coccolith Sr/Ca as a new indicator of coccolithophorid calcification and growth rate. Geochemistry, Geophysics, Geosystems 1. doi:10.1029/1999gc000015.

Tierney, J.E., Tingley, M.P., 2014. A Bayesian, spatially-varying calibration model for the TEX86 proxy. Geochimica et Cosmochimica Acta 127, 83–106. doi:10.1016/j.gca.2013.11.026.

Tierney, J.E., Tingley, M.P., 2018. BAYSPLINE: A New Calibration for the Alkenone Paleothermometer. Paleoceanography and Paleoclimatology 33, 281–301. doi:10.1002/2017PA003201.

de Vargas, C., Aubry, M.P., Probert, I., Young, J., 2007. Origin and Evolution of Coccolithophores. From Coastal Hunters to Oceanic Farmers. Elsevier Inc. doi:10.1016/B978-012370518-1/50013-8.

Ward, L.M., Shih, P.M., 2019. The evolution and productivity of carbon fixation pathways in response to changes in oxygen concentration over geological time. Free Radical Biology and Medicine 140, 188–199. doi:10.1016/j.freeradbiomed.2019.01.049.

Wilkes, E.B., Carter, S.J., Pearson, A., 2017. CO_2-dependent carbon isotope fractionation in the dinoflagellate Alexandrium tamarense. Geochimica et Cosmochimica Acta 212, 48–61. doi:10.1016/j.gca.2017.05.037.

Wilkes, E.B., Lee, R.B., McClelland, H.L., Rickaby, R.E., Pearson, A., 2018. Carbon isotope ratios of coccolith–associated polysaccharides of Emiliania huxleyi as a function of growth rate and CO_2 concentration. Organic Geochemistry 119, 1–10. doi:10.1016/j.orggeochem.2018.02.006.

Wilkes, E.B., Pearson, A., 2019. A general model for carbon isotopes in red-lineage phytoplankton: Interplay between unidirectional processes and fractionation by RubisCO. Geochimica et Cosmochimica Acta 265, 163–181. doi:10.1016/j.gca.2019.08.043.

Witkowski, C.R., Agostini, S., Harvey, B.P., van der Meer, M.T.J., Sinninghe Damsté, J.S., Schouten, S., 2019. Validation of carbon isotope fractionation in algal lipids as a CO_2 proxy using a natural CO_2 seep (Shikine Island, Japan). Biogeosciences 16, 4451–4461. doi:10.5194/bg-16-4451-2019.

Witkowski, C.R., van der Meer, M.T., Blais, B., Sinninghe Damsté, J.S., Schouten, S., 2020. Algal biomarkers as a proxy for pCO_2: Constraints from late quaternary sapropels in the eastern Mediterranean. Organic Geochemistry 150, 104123. doi:10.1016/j.orggeochem.2020.104123.

Witkowski, C.R., Weijers, J.W.H., Blais, B., Schouten, S., Sinninghe Damsté, J.S., 2018. Molecular fossils from phytoplankton reveal secular pCO_2 trend over the Phanerozoic. Science Advances 4. doi:10.1126/sciadv.aat4556.

Young, J., P.R., B., J.A., L., 2017. Nannotax3 website. International Nannoplankton Association. URL: http://www.mikrotax.org/Nannotax3.

Young, J.R., 2003. Biomineralization Within Vesicles: The Calcite of Coccoliths. Reviews in Mineralogy and Geochemistry 54, 189–215. doi:10.2113/0540189.

Zeebe, R.E., Wolf-Gladrow, D., 2001. CO_2 in seawater: Equilibrium, Kinerics,Isotopes. Elsevier oceanography series 65, 1–341.

Zhang, Y.G., Henderiks, J., Liu, X., 2020. Refining the alkenone-pCO_2 method II: Towards resolving the physiological parameter 'b'. Geochimica et Cosmochimica Acta 281, 118–134. doi:10.1016/j.gca.2020.05.002.

Zhang, Y.G., Pagani, M., Liu, Z., Bohaty, S.M., Deconto, R., 2013. A 40-million-year history of atmospheric CO_2. Philosophical Transactions of the Royal Society A: Mathematical, Physical and Engineering Sciences 371. doi:10.1098/rsta.2013.0096.

Declaration of interests

☒ The authors declare that they have no known competing financial interests or personal relationships that could have appeared to influence the work reported in this paper.

☐ The author is an Editorial Board Member/Editor-in-Chief/Associate Editor/Guest Editor for *[Journal name]* and was not involved in the editorial review or the decision to publish this article.

☐ The authors declare the following financial interests/personal relationships which may be considered as potential competing interests: